International Journal of Hydrogen Energy 80 (2024) 1046–1061

Contents lists available at ScienceDirect

International Journal of Hydrogen Energy

journal homepage: www.elsevier.com/locate/he

Material modeling for numerical simulation of elastomer O-rings with experimental verification at low temperatures

C. Repplinger [a,*], S. Sellen [b], S. Kedziora [a], A. Zürbes [c], S. Maas [a]

[a] University of Luxembourg, FSTM, Campus Kirchberg, 6, Rue Richard Coudenhove-Kalergi, L-1359, Luxembourg
[b] ROTAREX S.A., 24, Rue de Diekirch, L-7440, Lintgen, Luxembourg
[c] University of Applied Sciences BINGEN, Berlinstraße 109, 55411, Bingen am Rhein, Germany

ARTICLE INFO

Handling Editor: Z Sun

Keywords:
Elastomer O-Ring seal
High-pressure hydrogen storage
Primary leakage
Low temperature
Viscoelastic
Limited recovery

ABSTRACT

Elastomer O-ring seals are used in many technical applications and their requirements are becoming increasingly challenging for high-pressure applications like hydrogen storage systems. We analyze the performance of such seals at low temperatures and highlight the essential effects of primary leakage. Linear viscoelastic material modeling is described and defined with the help of Dynamic Mechanical Thermal Analysis (DMTA), Time-Temperature Superposition Principle (TTSP), and the shift function of Williams-Landel-Ferry (WLF) by assuming thermo-rheological simple material behavior. Numerical calculations and experimental validation are done for strain-rate dependent uniaxial tensile tests, Temperature Retraction (TR), Compression Set (CS), and specific leakage tests with O-rings. Thanks to Finite Element Analysis (FEA) it is possible to identify the most significant influences on the sealing tightness. Thermal shrinkage and the increasingly limited recovery of elastomer O-rings are mainly responsible for primary leakage at low temperatures and can be enforced by time-temperature dependent stress relaxation and manufacturing tolerances.

1. Introduction

O-rings are the most commonly used sealing type due to their simple manufacturing, versatility [1], high elastic deformability and resilience. They separate two different and at least one operative volume [2]. These volumes can contain equal or different media [3] with different load pressures. Several effects can induce material exchange [4], but a high difference in pressure is primarily responsible when acting with gases or fluids in valves, fittings, regulators or control blocks. The European Commission regulation [5] asks for a limited hydrogen leakage rate of 10 ml/h at −40 °C and 875 bar (1.25 times NWP). Hydrogen is heating while expanding and cooling during compression [6], which is known as Joule-Thomson effect [7] with a negative coefficient for hydrogen [8]. These are challenging technical requirements, especially for the elastomer O-rings that need always to ensure safe operation.

High-pressure gaseous hydrogen valve-tank systems require a compact design for Fuel Cell Electric Vehicles (FCEV). This technology must resist a high nominal working pressure (NWP) up to 700 bar and a huge temperature range from +85 °C to −40 °C simultaneously where low temperatures are considered as most critical for elastomer seals. A multifunctional on-tank valve (OTV) is directly connected to each high-pressure tank to control the hydrogen flow and enables the fill-up, storage, and supply of the fuel cell. The fuel cell unit generates electricity from hydrogen and oxygen, and the power control unit controls charging the battery and supplying the electric motor with the required voltage. Finally, the electric motor drives the zero-emission FCEV. The FCEV, the OTV, and the transparently visualized valve body with all elastomer O-rings are shown in Fig. 1. All red O-rings are loaded with high pressure, whereas the black ones are not pressurized but protect the valve from environmental influences. The O-rings do not experience dynamic lateral or radial movements.

Generally, two different leakages are defined, the first as primary leakage along the contact surfaces between the seal and its counter contacts and secondary leakage through the sealing material (permeation/diffusion). This work focuses only on primary leakage. The contact pressure between the O-ring and its counter surface must equal or exceed the operating pressure for all operating conditions to ensure a leak-proof and safe system. One of the most fatal accidents caused by such dysfunction of an O-ring seal due to primary leakage was the space shuttle Challenger disaster on January 28, 1986 where seven people died due to the limited resilience of an O-ring of the solid rocket booster at low ambient temperature that led to out-streaming of

* Corresponding author.
E-mail address: christian.repplinger89@gmail.com (C. Repplinger).

https://doi.org/10.1016/j.ijhydene.2024.06.427
Received 31 January 2024; Received in revised form 7 June 2024; Accepted 30 June 2024
Available online 19 July 2024

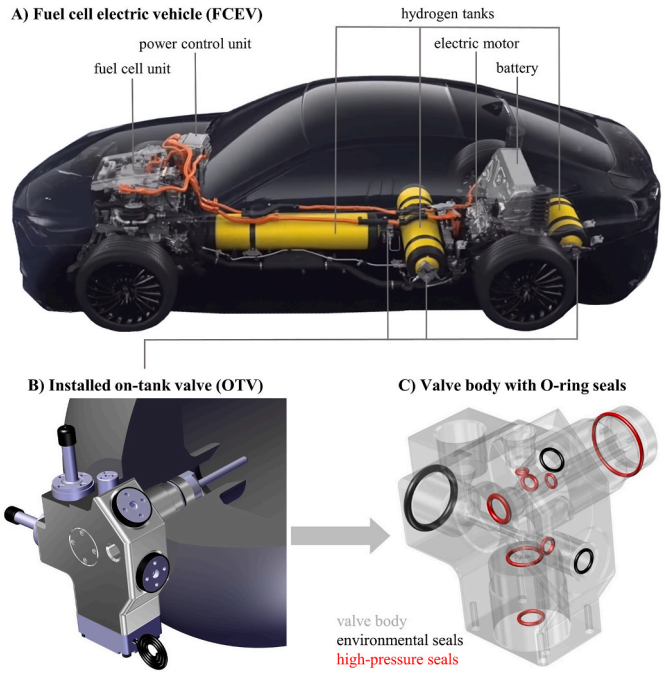

Fig. 1. A) Fuel Cell Electric Vehicle (FCEV) related to Ref. [9] with B) schematically installed OTVs and C) valve body with O-ring seals.

hot gas ("Blowby") and finally ended with an explosion of the space shuttle [10,11]. This well-known accident highlights the severe consequences of using a simple O-ring seal out of its functional capability. Therefore, it is important to know the materials limitations and identify the essential effects responsible for leakage at low temperatures, especially when working with high-pressure applications. In this article, detailed material modeling for elastomers is described and used for several numerical simulations that are validated by experiments. The significant effects responsible for primary leakage at low temperature are identified and Finite Element (FE) simulation allows us to model primary leakage at low temperature. All these results generate a better understanding of low-temperature sealing applications, e.g. hydrogen storage.

2. Material modeling

A traditional method to evaluate elastomer seals is testing under maximum required conditions. However, pure testing can be time-consuming and does not answer the question of how the material behaves under specific conditions and why leakage occurs. Developing new sealing materials and systems must address these questions early in development. Therefore, it is important to understand the material behavior and the most significant effects leading to leakage. Numerical simulations are very beneficial for identifying and analyzing these effects, but require a sufficient material model. Several basic material tests are needed to generate and evaluate an adequate material model that can be used for finite elem ent analyses (FEA).

2.1. Linear elasticity

A linear-elastic approach is not sufficient to give an accurate material description of an elastomer seal with high technical requirements. However, the approaches by Battermann and Köhler [12], and Lutz [13] based on the materials' shore hardness A and can be used for very rough estimations but are not sufficient to analyze the sealing behavior at low temperatures and the generation of primary leakage.

2.2. Hyperelasticity

Most highly elastic polymers, such as elastomers, have hyperelastic material behavior. Hyperelasticity is a non-linear material behavior according to structural mechanics when the relationship between stress and strain is non-linear but still elastic to more than 100% strain. Hyperelastic materials are normally considered incompressible and assume the original shape when unloading. Elastomers allow high deformations and because of this, they require different material tests for a full description of the material model. Uniaxial, biaxial, and pure shear tests are essential to characterize the mechanical material behavior in detail. Hyperelastic theory and modeling are described in technical literature by Holzapfel [14], Bonet and Wood [15] and Stommel et al. [16]. Hyperelastic material behavior is described with the strain-energy function W which is mostly expressed as a polynomial function and depends on the three deformation invariants $I_{1\text{-}3}$ based on three-dimensional elongations. The stretch λ_i presents the length ratio at the applied load to the original length.

$$\lambda = \frac{L}{L_0} = \frac{L_0 + dL}{L_0} = 1 + \varepsilon_{eng} \tag{1}$$

I_1 specifies the elongation of the space diagonal, I_2 presents the change of surfaces and I_3 describes the change of volume in a cubic element.

$$I_1 = {\lambda_1}^2 + {\lambda_2}^2 + {\lambda_3}^2 \tag{2}$$

$$I_2 = {\lambda_1}^2{\lambda_2}^2 + {\lambda_2}^2{\lambda_3}^2 + {\lambda_1}^2{\lambda_3}^2 \tag{3}$$

$$I_3 = {\lambda_1}^2{\lambda_2}^2{\lambda_3}^2 \tag{4}$$

The most significant hyperelastic models and their strain-energy functions are listed in the following[17–22].

$$\text{Neo} - \text{Hooke} : W = C_{10}(I_1 - 3) + \frac{1}{D_1}(J-1)^2 \tag{5}$$

$$\text{Mooney} - \text{Rivlin} : W = C_{10}(I_1 - 3) + C_{01}(I_2 - 3) + \frac{1}{D_1}(J-1)^2 \tag{6}$$

$$\text{Yeoh} : W = \sum_{i=1}^{n} C_{i0}(I_1 - 3)^i + \sum_{k=1}^{n} \frac{1}{D_1}(J-1)^{2k} \tag{7}$$

$$\text{Ogden} : W = \sum_{i=1}^{n} \frac{2\mu_i}{\alpha_i}({\lambda_1}^{\alpha_i} + {\lambda_2}^{\alpha_i} + {\lambda_3}^{\alpha_i} - 3) + \sum_{k=1}^{n} \frac{1}{D_1}(J-1)^{2k} \tag{8}$$

$$\text{Gent} : W = -\frac{\mu J_m}{2} ln\left(1 - \frac{I_1 - 3}{J_m}\right) + \frac{1}{D_1}\left(\frac{J^2 - 1}{2} - lnJ\right) \tag{9}$$

Each strain energy function is separated into one deviatoric and one volumetric part. The deformation invariants I_i, the limiting value J_m and the material constants C_{ij}, μ_i and α_i are part of the deviatoric strain-energy, where the elastic volume ratio J and the incompressibility factor D_1 describe the volumetric change.

$$J = \sqrt{I_3} = \lambda_1\lambda_2\lambda_3 = \frac{V}{V_0} \tag{10}$$

$$D_1 = \frac{2}{K} \tag{11}$$

$$K = -V\frac{dp}{dV} = \frac{E}{3 - 6\nu} \tag{12}$$

The last term of equation (12) is only valid for isotropic materials and gives the relation to the Poisson's ratio ν. Most elastomer materials do not have noticeable volume changes and can be assumed incompressible ($\nu = 0.5$) so that only isochoric motions are possible [14]. Therefore, the last term of equations (5)–(9) can be neglected for incompressible

material behavior. Fillers and Tschoegl [23], as well as Moonan and Tschoegl [24,25] investigated the pressure-dependency of viscoelastic mechanical material behavior. They developed a model based on the time, temperature, and pressure superposition principle [26]. Ferry [27] gives a detailed description of this pressure dependency, and Ho [28] describes the shift of the glass transition temperature at high pressure. However, we use the incompressible approach for the further procedure.

At least uniaxial stress-strain test data are necessary to evaluate a sufficient hyperelastic model for the strain range of interest. Fig. 2 shows the uniaxial test data of five specimens made of 80 FVMQ 567. We selected this material as it shows good evaluation testing characteristics and reaches its functional capability under highly severe conditions (low temperature + high pressure) that will be presented later. The specimens' geometry and the test procedure follow DIN ISO 37 [29]. These uniaxial tests were performed at O-Ring Prüflabor Richter GmbH with Zwick/Roell zwicki Retroline (2.5 kN).

The uniaxial test results in Fig. 2 show a good correlation and an elongation at break of approximately 124 %. Next, the arithmetic mean value curve is fitted with several hyperelastic material models for the expected strain range ($\varepsilon_{max} \approx 60$ %). Fig. 3 provides a visual comparison of these models to the experimental data. The individual models are fitted to the test data curve by minimizing the Frobenius norm of the relative errors when comparing the hyperelastic model and the test curve.

$$\|X\|_F = \sqrt{\sum_{i=1}^{n} |dev_{rel}|^2} \tag{13}$$

All hyperelastic models match well for a strain range of up to 40 %. The Ogden model generates the best fit; however, the simple Neo-Hookean material model gives a sufficient fit, so we continue with this model. The curve fitting process is implemented in most numerical software and enables the generation of the parameters for several hyperelastic material models.

The hyperelastic material model presents a more realistic description of the mechanical material behavior of elastomers than a pure linear-elastic approach and can be sufficient for analyses in several applications. However, a pure hyperelastic material model does not consider the influences of time and temperature, which must be considered for an adequate analysis of the most significant influences on sealing behavior, especially for low-temperature applications. Therefore, we continue with the viscoelastic material modeling that is added to hyperelasticity.

2.3. Viscoelasticity

Viscoelastic material behavior exhibits liquid-like and solid-like characteristics. For infinitesimal strains, most solids approach Hooke's law [30] to describe elastic behavior, whereas many liquids approximate Newton's law [31] to present viscous material characteristics [27]. A simple viscoelastic model exhibits both a spring as an elastic element and a dashpot as a viscous element when undergoing deformations. Therefore, viscoelastic materials have a time-dependent behavior that can be described by different models, which present a combination of Hookean elastic springs and Newtonian viscous dashpots in series, parallel, or mixed arrangement to establish this complex material behavior [32]. The simplest mechanical viscoelastic models are a combination of one spring

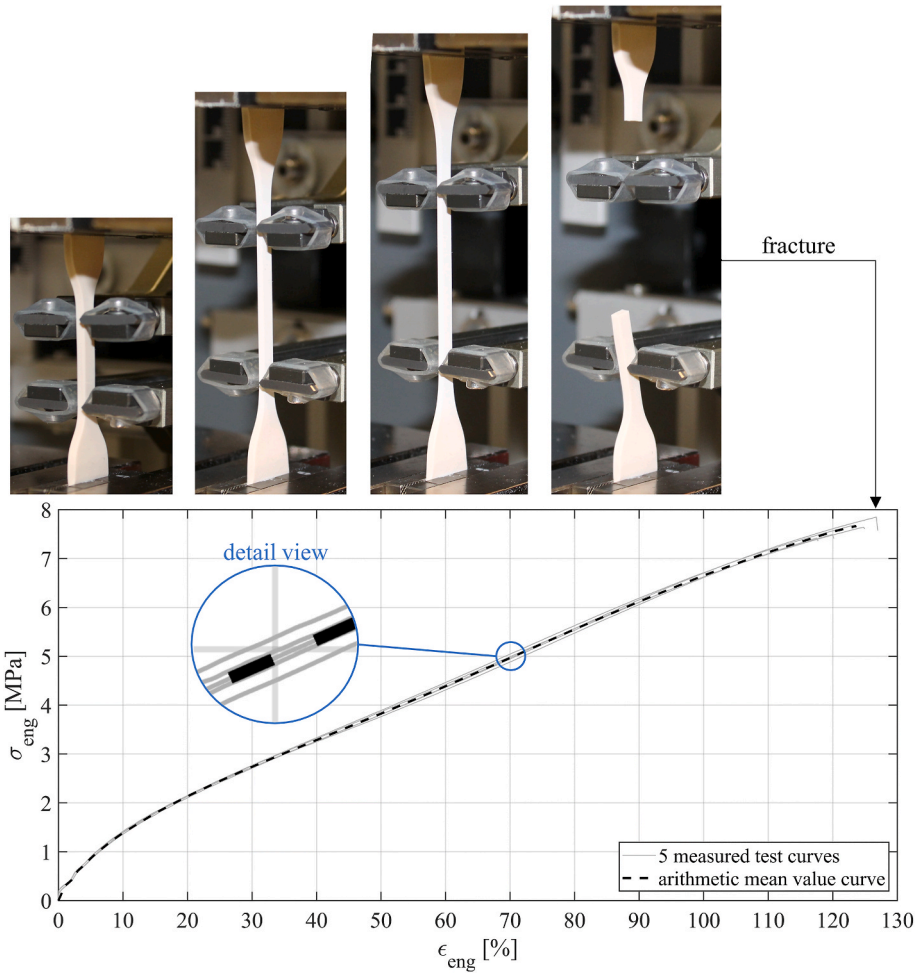

Fig. 2. Measured stress-strain curve of 80 FVMQ 567.

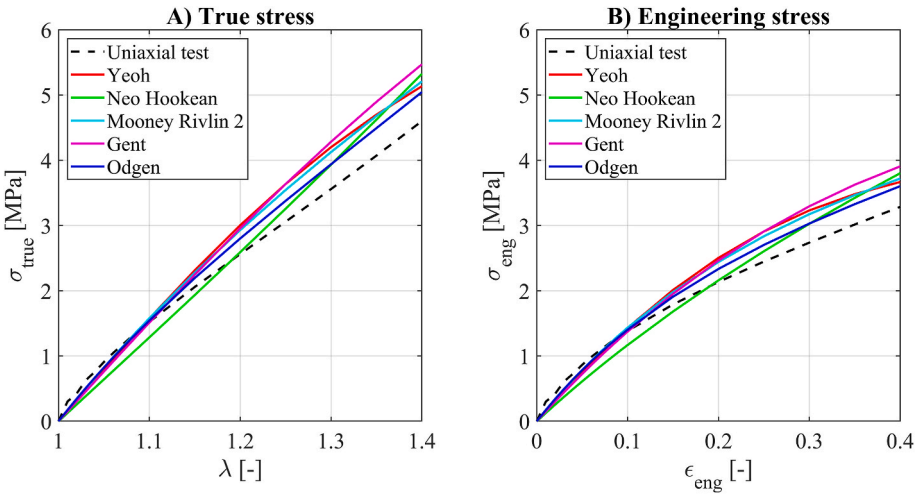

Fig. 3. Curve fit of several hyperelastic models to the uniaxial test data of 80 FVMQ 567 with A) true stress and B) engineering stress.

and one dashpot, either in parallel (Kelvin-Voigt model) or in series (Maxwell model) [33]. Viscoelastic equations can be formulated in terms of the deformation type, e.g. simple extension, shear, or bulk compression, but analogous relations exist for them (E, G, K) [27]. Kelly [34], Hearn [35], and Rust [36] give a detailed description of the two basic viscoelastic models:

$$\text{Kelvin} - \text{Voigt model} : \sigma = E\varepsilon + \eta\dot{\varepsilon} \tag{14}$$

$$\text{Maxwell model} : \dot{\varepsilon} = \frac{\dot{\sigma}}{E} + \frac{\sigma}{\eta} \tag{15}$$

where E is the modulus of elasticity and η is the viscosity. Almost constant strain conditions are given for installed O-ring seals, which is why the Kelvin-Voigt model behaves like a purely linear elastic solid, and the Maxwell model describes stress relaxation under constant strain.

$$\text{When } \varepsilon = \text{const} : \dot{\varepsilon} = \frac{d\varepsilon}{dt} = 0 \tag{16}$$

$$\text{Kelvin} - \text{Voigt model} : \sigma = E\varepsilon \tag{17}$$

$$\text{Maxwell model} : \sigma = \sigma_0 e^{-\left(\frac{E}{\eta}\right)t} \tag{18}$$

Viscoelastic material behavior generally depends on the strain rate and temperature. Higher strain rates lead to stiffer material behavior, and lower strain rates generate softer behavior. Contrary, the material behaves stiffer at lower temperatures and softer at higher temperatures. This means the material behaves similarly at high temperatures as in low strain rates, and the reverse is also true [16]. The Time-Temperature Superposition Principle (TTSP) uses this relation and was presented by Tobolsky [37]. TTSP enables a simple transformation of viscoelastic data from one temperature to another as well as changes in the time or frequency domain.

The Dynamic Mechanical Thermal Analysis (DMTA) is a typical measurement technique used to define viscoelastic material properties by applying TTSP. DMTA generates a sinusoidal load and measures the viscoelastic response of the material as phase angle δ between strain and stress and the complex moduli E* to calculate the storage modulus E′, loss modulus E″, and loss factor tanδ.

$$\delta = 2\pi f \Delta t \tag{19}$$

$$E' = E^* \cos\delta \tag{20}$$

$$E'' = E^* \sin\delta \tag{21}$$

$$\tan\delta = \frac{E''}{E'} \tag{22}$$

Several isotherms are needed to make use of TTSP and DMTA performs frequency sweeps for each isotherm. When applying an oscillating strain, stress is exactly in phase with strain for a perfectly elastic solid or 90 ° out of phase for a perfectly viscous liquid [38]. Viscoelasticity describes the state somewhere in between and includes a stored and a dissipated part of energy in each cycle. If the magnitude and rate of strain are infinitesimal, and linear differential equations with constant coefficients can describe the time-dependent stress-strain relation, it is called a linear viscoelastic behavior. Here, the ratio of stress and strain is only a function of time or frequency and not of stress magnitude [39]. Therefore, the strain also alternates sinusoidally but out of phase to the load [27]. Stress relaxation measurement in the frequency domain can be used, as the TTSP implies that time or frequency is equivalent to temperature [40–42], and both generate time- and temperature-dependent material data that are used for the following procedure.

First, a reference temperature is defined and this isothermal data set is fixed. Afterward, an appropriate horizontal shifting along a logarithmic frequency scale of all the other individual isothermal relaxation measurements generates one continuous curve [43]. This curve is known as the master curve and describes the viscoelastic material behavior for a wide time- or frequency range of the reference temperature and can be shifted to each temperature of interest. This horizontal shift along the logarithmic time axis is done with the time-temperature shift factor a_T:

$$a_T = \frac{t_T}{t_{T_{ref}}} = \frac{f_{T_{ref}}}{f_T} \tag{23}$$

where t_T is the needed time to give a certain response at the temperature T and t_{Tref} is the time needed to give the same response at the reference temperature T_{ref}. Likewise, the shift factor can be determined along the logarithmic frequency scale where f_T is the necessary frequency to reach a specific response at temperature T and f_{Tref} is the frequency at reference temperature to achieve the same response of the material [41].

The most recognized shift factor that links the master curve to its reference temperature was established by Williams, Landel, and Ferry [44] and is also known as the WLF shift function shown in equation (24) [27,41].

$$\text{WLF} - \text{shift} : \lg(a_T) = \frac{-C_1(T - T_{ref})}{C_2 + (T - T_{ref})} \tag{24}$$

The resulting full master curve includes viscoelastic information that

is not feasible to measure by experiments but can be defined by TTSP [1]. Measurement techniques over time [37,40,45–48] or over frequency [1,11,16,49,50] can be found in numerous technical publications. The principle DMTA measurement method and the master curve generation are presented in Fig. 5. It shows the DMTA, the master curve generation with the shift factor a_T, as well as the shift of the master curve to each temperature of interest. Clear changes in the moduli can be seen around the so-called glass transition temperature T_g, which is a significant thermo-physical value for polymeric sealing materials concerning their operating temperature range. Below T_g, the oscillating molecules come to rest, and their intermolecular attractive forces are in full effect. This leads to greater strength and hardness in the material [51]. The shape of the molecules is not altered, and the material is in a hard, brittle, glassy state [40]. At and above T_g, the mechanical material behavior changes from glassy to rubber-like, and the reverse is true below. When increasing the temperature above T_g, the molecular motion starts again [52], and the E-modulus is clearly reduced.

The elasticity of elastomers relies on the elasticity of each polymeric chain. A single chain consists of connected rigid elements that can be moved in relation to each other. This movement is highly dependent on thermal energy. If a polymeric chain is stretched and its ends are held, the thermal movements of the elements generate a force that pulls the ends toward the inside. The intensity of the elasticity depends on this thermal movement, which is proportional to the absolute temperature. Hence, the elastic recovery force is also proportional to the absolute temperature and causes contraction in the chain. It has to be mentioned that the temperature influences the intensity of the force, but not its direction. The recovery force is weakened proportionally when decreasing the temperature until reaching the glass transition temperature T_g. The chains freeze and the thermal movement comes to rest when cooling below T_g. Consequently, the recovery force is disproportionately weakened. Elastomers are not made of one singular chain; instead, they consist of three-dimensional, randomly coiled molecular chains [53]. Rubber chains are always associated with branches and loose chains dependent on filler systems used. However, a singular chain gives a simplified explanation of the elastomer's temperature-dependent elasticity, as presented in Fig. 4.

At room temperature, the thermal movements are active, and a recovery force of the chain is given when applying a load. Here, a fast recovery to the original, preferred state is directly given when unloading the chain (see Fig. 4A). For lower temperatures above T_g, the thermal movements are limited, but sufficient to bring the chain slowly back to its preferred state when unloading (see Fig. 4B). Below T_g, there are no thermal movements, so the material loses its entropy-driven elasticity [54] and no recovery force is given. Therefore, the chain is totally frozen and does not recover when the load is released (see Fig. 4C). Consequently, elastomers must be used above T_g to ensure the functional capability of the seal. T_g can be determined using different methods, such as DMTA or Differential Scanning Calorimetry (DSC) [55]. Elastomers start to lose their rubbery properties when the declining temperature approaches T_g. Elastomeric seals become progressively less able to seal and leakage may occur because of stiffening and thermal shrinkage [28].

Fig. 5A presents the principal DMTA measurement technique and the subsequent methods leading to a master curve (B) that can be shifted to each temperature of interest (C).

The DMTA measures the reacting force and its phase displacement to the given sinusoidal strain. The stress also shows a sinusoidal run but out of phase. The storage modulus E' is calculated and presented in (B) with its measured data in the green frequency range (0.1–30Hz). T_3 is also set as the reference temperature, and the other isotherms are shifted to one continuous master curve. This master curve can be shifted to each temperature of interest and presents an almost complete frequency range. This master curve needs to be described mathematically. Generally, a Maxwell model is appropriate to describe stress relaxation, but one element is insufficient to achieve an accurate correlation. Therefore, several Maxwell elements and one spring in a parallel arrangement are used for the modeling of stress relaxation in viscoelastic materials like elastomers.

This arrangement is termed Prony-series and is visualized in Fig. 6. It defines the time- and temperature-dependent modulus in equation (25), and equation (26) shows the complex moduli in the frequency domain. The Prony-series is commonly used to model linear viscoelastic material behavior and is implemented in many finite element analysis software [48].

$$E(t,T) = E_0\left[1 - \sum_{i=1}^{N} e_i\left(1 - e^{\frac{t}{\tau_i a_T}}\right)\right] = E_\infty + \sum_{i=1}^{N} E_i e^{\frac{t}{\tau_i a_T}} \tag{25}$$

$$E^*(\omega,T) = E_0\left[1 - \sum_{i=1}^{N} e_i \frac{1}{1 + (\tau_i a_T)^2\omega^2}\right] = E_\infty + \sum_{i=1}^{N} \frac{E_i \omega^2 (\tau_i a_T)^2}{1 + \omega^2(\tau_i a_T)^2} \tag{26}$$

The relaxation times τ_i capture the strain rate sensitivity and strain history dependence [56]. This ratio of viscosity η_i and the elastic modulus E_i defines the restoring behavior of a Maxwell-element that relaxes proportionally to $e^{-t/\tau i}$ [32]. Furthermore, e_i presents the relative relaxation strength and is known as the relaxation coefficient.

$$\tau_i = \frac{\eta_i}{E_i} \tag{27}$$

$$e_i = \frac{E_{i-1} - E_i}{E_0} = \frac{\Delta E_i}{E_0} \tag{28}$$

The shift factor a_T transforms the relaxation times, shifting the master curve on the logarithmic time or frequency axis to the temperature of interest. The relaxation times τ_i and the relaxation coefficient e_i present the Prony-parameters essential for the final material model. Furthermore, the relaxation times τ_i always appear in the combination $t/\tau i$ for the time domain and $\omega\ \tau i$ for the frequency domain as further detailed by Popov [57]. Kraus et al. [58] showed that the time-dependent relaxation properties of a material can be transferred to

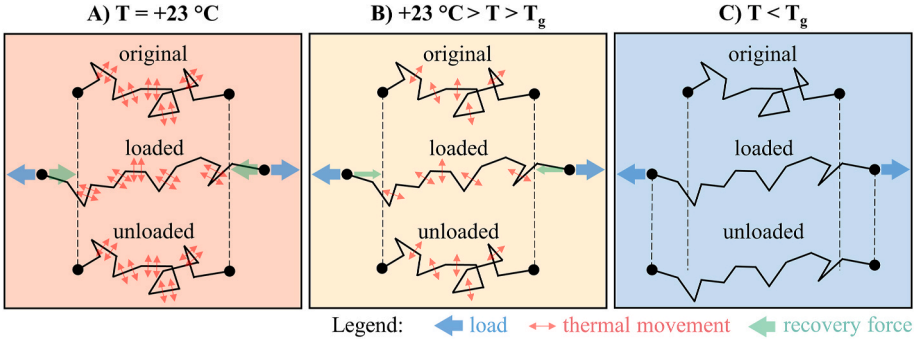

Fig. 4. Simplified singular chain at: A) T = +23 °C; B) +23 °C > T > T_g; C) T < T_g.

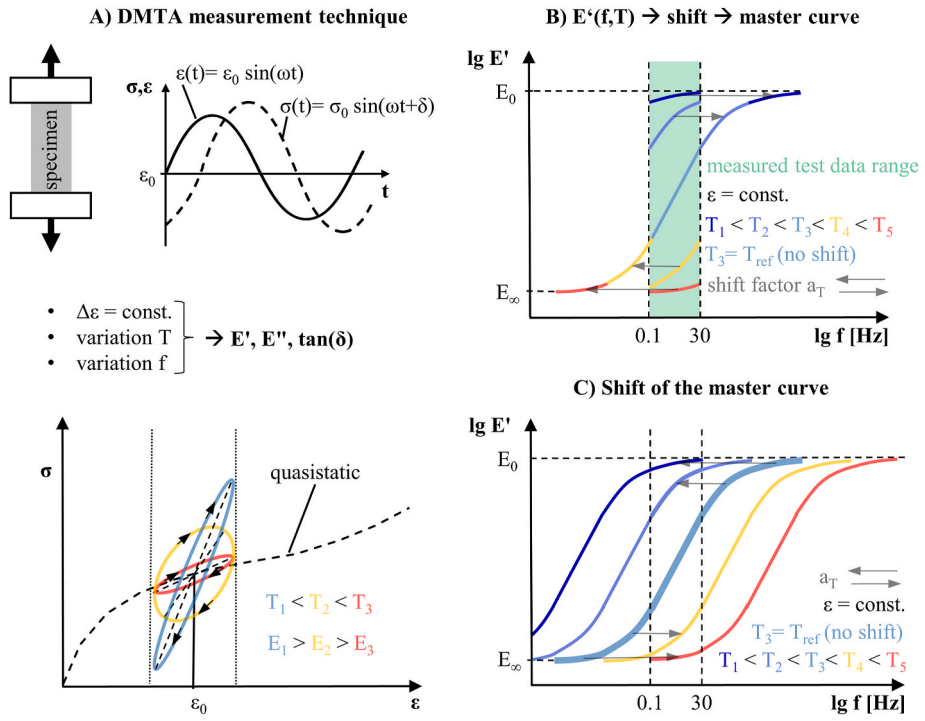

Fig. 5. A) DMTA measurement technique with B) master curve generation and C) shift.

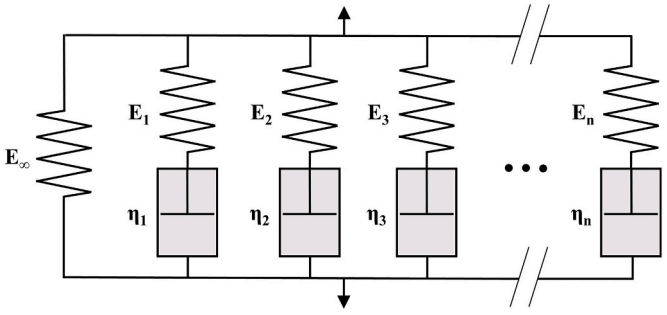

Fig. 6. Prony-series.

the frequency-dependent complex modulus and vice versa via Fourier transformation. Consequently, both techniques finally lead to the same result, the Prony-series.

If the change of temperature is completely equivalent to a shift along the logarithmic time scale, the material is called Thermo-Rheologically Simple (TRS) [33,59]. This means that all relaxation times of the spectrum can be transformed for each temperature of interest. Most polymers do not present perfect TRS behavior, but this procedure can provide a sufficient approach.

In this work, DMTA was used as previously described to finally determine the Prony-parameters.

We used a specimen with a rectangular cross section with a length of 7.6 mm, a width of 2 mm, and a thickness of 2.1 mm. Uniaxial DMTA-testing was done at O-Ring Prüflabor Richter with TA Instruments DMA 800, as shown in Fig. 7A. A frequency sweep was performed between 0.1Hz and 30Hz for each isotherm with the temperature range between −100 °C and +150 °C. The isothermal steps were defined as 10°C-steps at the maximum and minimum temperature limit, which were refined to 5°C-steps as the glass transition temperature approached. The transition temperature range was measured with 2°C-steps to give a more detailed description of the relevant changes in the viscoelastic material characteristics. Fig. 7 visualizes the measurement of the storage modulus E' (B), the loss modulus E'' (C), the complex modulus E* (D), as well as the loss factor tan δ (E) over the temperature range.The measured data in Fig. 7 present the frequency sweep of each isotherm and give information about the influence of the strain rate and temperature on the material behavior. There is no significant change of the individual isothermal values for higher temperatures above room temperature and very low temperatures far below T_g when considering the frequency sweep. This presents almost completely relaxed material behavior for higher temperatures or glass-like behavior at very low temperatures. The glass transition temperature T_g is defined as −60 °C for 80 FVMQ 567 by the manufacturer, and the test results confirm this and present the greatest viscoelastic changes of the material around T_g. At this temperature, the relaxation rates of the storage modulus are much higher, and both the loss modulus and the loss factor show higher magnitudes when changing the strain rate (frequency sweep). This means the material has a higher frequency (time) sensitivity around T_g.

We focus on the storage modulus E' (see Fig. 8A) in order to generate an accurate master curve by using the WLF-shift factor as visualized in Fig. 8B. Therefore, we set T_g as the reference temperature and shifted all the other isotherms to a continuous master curve as shown in Fig. 8C. In this analysis, the WLF-parameters generated the best fit with $C_1 = -24$ and $C_2 = 120$ °C.

Fig. 8A shows the data set as storage modulus for isotherms over frequency. It is apparent that the isothermal data around T_g present the greatest changes in the storage modulus, as discussed before, where higher frequencies show stiffer, and lower frequencies softer, material behavior. The generated master curve was transferred as a data set to the software ViscoData, which enables the definition of the Prony-series. 30 elements gave a representative mathematical description of the master curve. The relaxation times τ_i and relaxation coefficients e_i present the Prony-parameters and describe the discrete relaxation spectrum that is shown in Table 1.

The defined Prony-parameters and the reference temperature for TTSP with its WLF-factors were implemented into the numerical material model in addition to the hyperelastic material model. This final material model combines hyperelasticity (Neo-Hooke) and viscoelasticity (Prony-series, TTSP, WLF) in order to describe the time- and

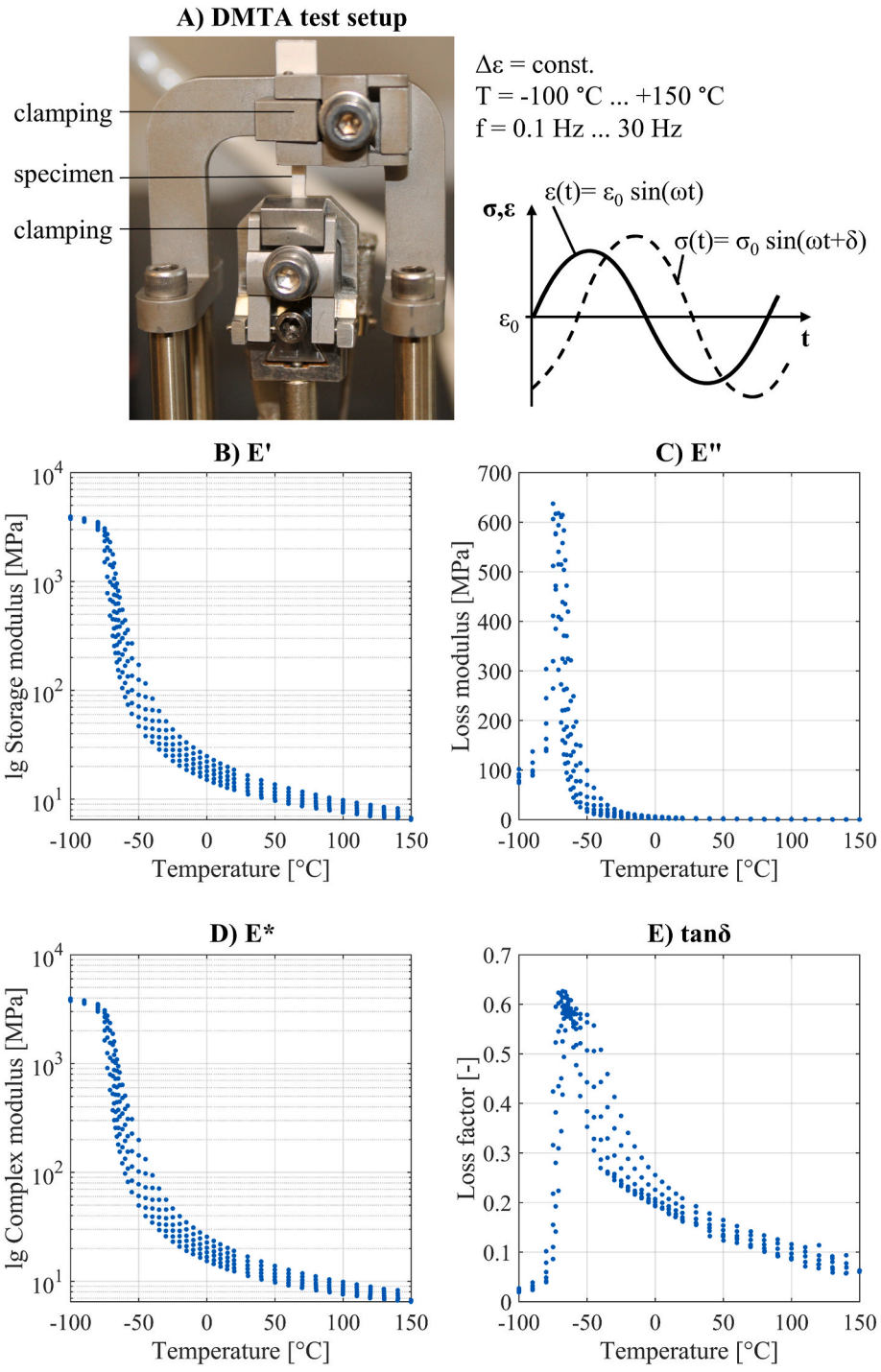

Fig. 7. A) DMTA test setup and viscoelastic measured data of 80 FVMQ 567 with frequency sweeps over temperature for: B) storage modulus; C) loss modulus; D) complex modulus and E) loss factor.

temperature dependency of the material. We assume thermo-rheological simple (TRS) material behavior because a pure WLF-shift was able to generate an almost continuous master curve by using TTSP.

3. Experimental and numerical results

Technical requirements ask for a wide temperature range, so the consideration of the thermal expansion coefficient of the O-ring and its surround is definitely needed. The elastomer O-ring has a thermal expansion coefficient of 2.2 10^{-4}1/°C for 80 FVMQ 567, the housing 2.3 10^{-5}1/°C for EN AW 6061 T6, and the piston 1.3 10^{-5}1/°C for Inconel 718. Additionally, all FE simulations in this work were done with ANSYS Workbench and used the previously described hyper-viscoelastic material model.

3.1. Validation of the material model

This material model needs to be validated before further numerical analyses follow. Therefore, a tensile test at two different strain rates was performed to include the influence of time, and an additional temperature-retraction test was done to deliver the temperature dependency. Both experiments are compared to FEA results.

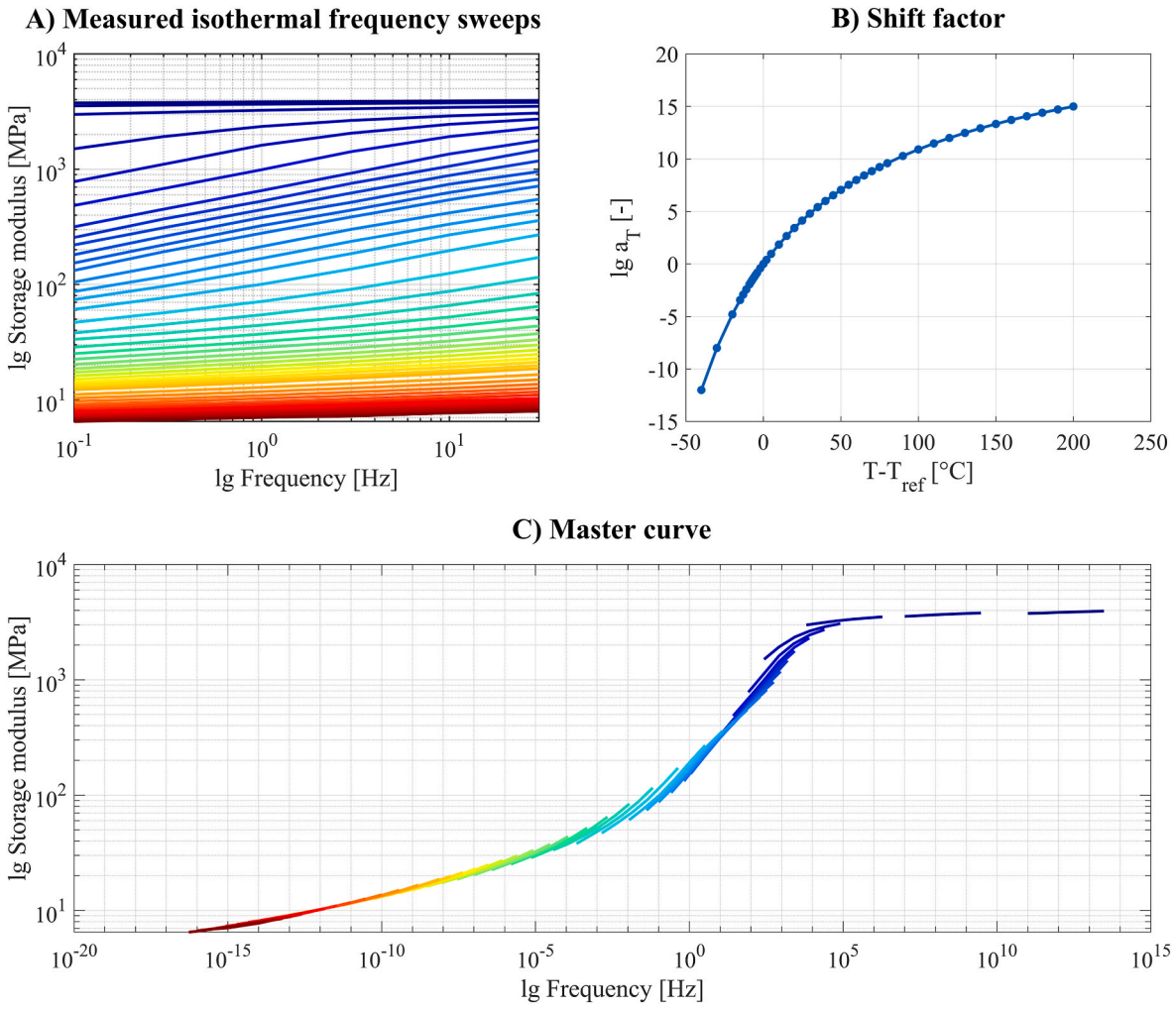

Fig. 8. Master curve generation with A) Measured isothermal storage modulus E′ curves; B) WLF shift factor and C) master curve.

3.1.1. *Strain-rate dependent uniaxial tests*

Fig. 9 presents the measured stress-strain curves of five samples with the strain rate 500 mm/min linked to ISO 37 [29], as well as one quasistatic curve with a strain rate of 0.6 mm/min. This quasistatic curve shows much lower stress values in comparison to the first five tests at 500 mm/min because the elastomer has time to restructure its chains, and stress relaxes to lower values. The numerical stress-strain results fit well with the real test data and highlight the time-dependent material behavior.

3.1.2. *Temperature-retraction test*

Furthermore, a Temperature-Retraction (TR10-70) test was done with three samples at O-Ring Prüflabor Richter GmbH to analyze the recovery of the material at low temperatures. The sealing manufacturer generally gives this value and describes the low-temperature capability of an elastomeric compression seal, e.g. O-rings. The experiment used three O-rings (15.6 mm × 1.78 mm) for the TR10-70 test as mentioned in ISO 2921 [60]. They were stretched up to 50 % strain at room temperature, cooled down to −71 °C, held for 10 min, and released to recover freely while the temperature was increased at 1 °C/min. The temperature corresponds to significant retraction values, e.g. 10 % (TR10) or 70 % (TR70) to describe the unfreezing process [28]. During this process, the component's length and retraction are measured. This can either be done with a typical uniaxial tensile test sample or an O-ring with a cross-sectional diameter between 1.5 mm and 4 mm [60], as given in our experiment. The TR10-value defines a temperature at which a specimen elongated by 25 % or 50 % retracts 10 % after load release. This value is among the most significant values for O-ring applications at low temperatures. In practice, O-rings work from 10 to 15 °C below TR10. The lesser the temperature difference between TR10 and TR70, the faster the material regains its elasticity. The TR values can be defined as shown in equation (29):

$$TR = \left[\frac{(L_e - L_t)}{(L_e - L_0)}\right] 100\% \tag{29}$$

where L_0 is the length of the unstretched specimen, L_e is the length of the stretched specimen, and L_t is the length of the specimen at any observed temperature. The comparison of the three experimental curves and the numerically determined curve in Fig. 10 shows good agreement and presents the influence of temperature on the material behavior.

This evaluation process shows that this TRS visco-hyperelastic material model agrees with experimental results and is able to present time- and temperature-dependent material behavior, which is necessary for the numerical analysis of the significant effects influencing the sealing behavior, as presented in the following chapter.

3.2. *Significant low-temperature effects*

Several effects influence the sealing behavior at low temperature and are addressed in the following. Elastomer seals become stiffer as they cool, generally shrink more than their metal surrounding, limit their recovery, and slow their reaction to a load. This highlights the material's

Table 1
Prony-parameters.

moduli		
$E_0 = 3945$ MPa		$E_\infty = 6.5$ MPa
i	relaxation times τ_i [s]	relaxation coefficients e_i [−]
1	5.90519E+14	1.96671E-04
2	3.00337E+13	2.46413E-04
3	1.79459E+12	3.33589E-04
4	1.17341E+11	4.20208E-04
5	6.56673E+09	5.45029E-04
6	3.61005E+08	6.82540E-04
7	2.34672E+07	8.59601E-04
8	1.57685E+06	1.08844E-03
9	1.06435E+05	1.48297E-03
10	7.32324E+03	2.08406E-03
11	5.71279E+02	2.90767E-03
12	5.21386E+01	4.95884E-03
13	4.31830E+00	6.76300E-03
14	5.02112E-01	1.41177E-02
15	6.25617E-02	2.97415E-02
16	1.08874E-02	4.57924E-02
17	1.59530E-03	9.96380E-02
18	2.31943E-04	1.70736E-01
19	5.06548E-05	1.35157E-01
20	2.06534E-05	1.67180E-01
21	5.36303E-06	1.13916E-01
22	1.08336E-06	7.24675E-02
23	1.20787E-07	2.39695E-02
24	5.22409E-09	3.07005E-02
25	8.26243E-10	1.47417E-02
26	3.50110E-10	5.68723E-04
27	2.10883E-10	1.78770E-02
28	1.82532E-13	6.61736E-03
29	1.77914E-13	1.39925E-02
30	1.65447E-14	1.85773E-02

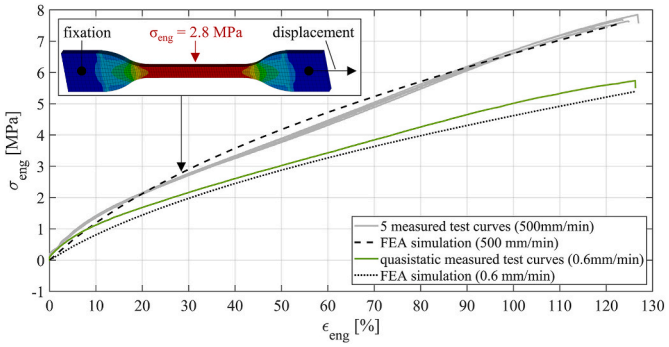

Fig. 9. Comparison of measured and simulated stress-strain curves for 80 FVMQ 567 at 23 °C.

time- and temperature dependency, which can be described with viscoelasticity. Below T_g, no recovery is given, and the load transfer is limited, which could lead to leakage at an elastomeric seal. Additionally, the shrinkage of the seal needs to be considered, and the material loses flexibility and may not match perfectly to the contrary sealing surface as it would at room temperature. The elastic recovery of elastomers is time- and temperature-dependent [61], and Akulichev et al. [49] showed that the leakage of an HNBR O-ring occurs at lower temperatures when a slower cooling rate is used. For an O-ring with 30 % compression, leakage occurred at −20 °C when cooling by 1 °C/s in comparison to a leakage temperature of −42 °C when cooling by 0.001 °C/s. Several studies by Jaunich et al. [11,62,63], Grelle et al. [54], and Akulichev et al. [49] explained the limited sealing behavior of elastomeric seals with thermal contraction and the loss of elasticity when cooling. Thermal contraction is generally compensated by the elastic recovery that prevents the generation of a gap at the sealing surface. If the recovery is insufficient at low temperatures, a gap develops, leading to leakage. The essential effects and their magnitude for primary leakage are analyzed in the following.

3.2.1. Machining tolerances

Every machining process has tolerances that must be considered for the piston, the cylinder and the O-ring. The machining tolerances of O-rings are defined in DIN ISO 3601-1 [64] for the relevant inside diameter d_1 and the cross section diameter d_2. The metal housing and the piston also have dimensional and surface tolerances depending on the requirements. It is very unlikely to have a worst-case tolerance combination in the real world. However, Fig. 11 highlights the change of contact pressure for a radial installed O-ring at 23 °C at nominal (A) and worst-case tolerances (B). The contact pressure is reduced by around 28 % at the outer diameter and 23 % at the inner diameter.

3.2.2. Thermal shrinkage

The elastomer O-ring has a clearly higher thermal expansion coefficient α_{th} with a factor by ca. 10 higher than the surrounding metal parts like housing and piston. Therefore, temperature changes influence the geometry of the seal and its housing, which can be shown with the material-dependent thermal expansion coefficient α_{th}.

$$\alpha_{th} = \frac{1}{l}\frac{dl}{dT} \tag{31}$$

This coefficient characterizes linear proportionality for the change of temperature and the resulting elongation of the material. α_{th} describes the linear thermal shrinkage when cooling and expansion when heating. Therefore, the elongation of a component depends on its length l, the temperature T, and the material-dependent thermal expansion coefficient α_{th} [65]. When cooling, linear proportional geometric changes are given, but it is not clear what the influence is on the contact pressure as elastic recovery must be given to counteract these geometrical changes.

3.2.3. Limited elastic recovery

In contrast to energy-elastic materials such as metals, elastomers have entropy-elastic material behavior. Entropy presents a degree of disorder, which is higher in the entangled, disordered state of the polymeric chains than in an arranged, orderly state. Above the glass transition temperature, the change in entropy is the driving force behind the resilience of elastomers [52]. From the thermodynamic perspective, a deformed elastomer tends to return to a state of lower potential molecular energy and higher disorder [66]. For a tension-loaded elastomer, the recovery force brings the chains back to their statistically preferred disorder when unloading. However, such chains are not compressed under a compression load, e.g. O-rings. Instead, they can only be formed to a different arrangement and are also stretched because the preferred disordered state of the elastomeric seal with its chains describes the highest compression level, and elastomers are considered incompressible. Therefore, the molecules spread vertically to the compression load. If there is a geometric limitation such as a notch, the elastomer proportionally transfers the compression load to the contact surfaces as given for a pressure-loaded O-ring. This brilliant ability is used for elastomeric sealing systems but is somehow limited at low temperatures.

The recovery of elastomers can be determined with the Compression Set (CS) using DIN ISO 815-2 [67]. This test is similar to the TR10-test, but considers compression load. Here, the specimen is compressed at room temperature, cooled down to the test temperature, then released again by plate 1 (see Fig. 12). The free recovery of the specimen is measured over time at a constant temperature. The compression set can be calculated as presented in equation (30) and is defined after 30 min:

$$CS = \left[\frac{(d_2 - d(t))}{(d_2 - d_c)}\right] 100\% \tag{30}$$

In this work, all O-rings (axial or radial) are simulated in a 2-dimensional axisymmetric model. The meshing of the seal and its contacts is refined

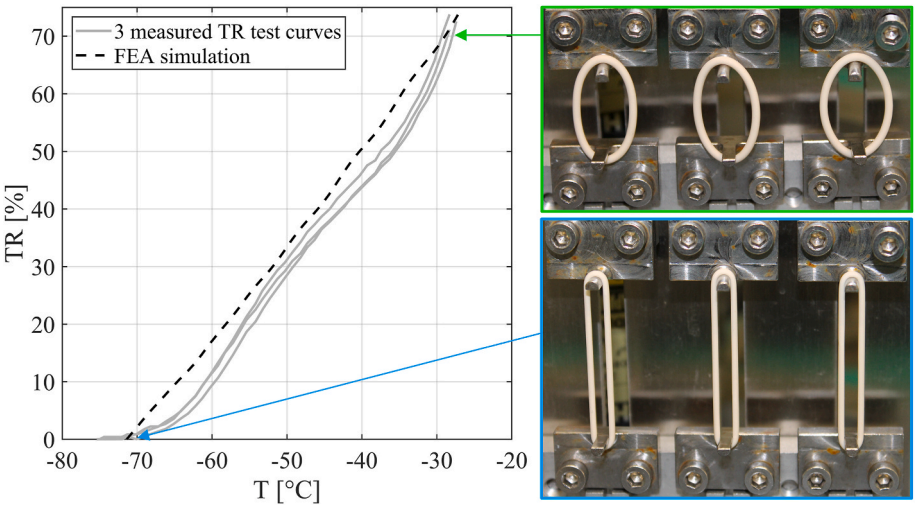

Fig. 10. Comparison of measured TR-tests with O-rings and FEA.

and uses quadrilateral dominant elements with quadratic element order (ANSYS element type: 183). The frictional coefficient is defined as 0.1 due to the high surface finish (Ra = 1.6 μm) and the fact that a greased O-ring does not move dynamically. Normal Lagrange contact formulation was used and did not allow penetration. An assembly and pressure-load are modeled, where the pressure is activated with fluid pressure penetration in ANSYS to generate a realistic acting pressure. A thermal condition is used to present temperature changes.

Fig. 12 illustrates CS at 23 °C (A), −40 °C (B), and −60 °C (C) for the 21 % compressed, axial O-ring 15.6 mm x 1.78 mm. At 23 °C (A), the seal shows a fast recovery close to its original shape with a compression set of 10.3 % after 30 min. At −40 °C, the recovery is limited and achieves CS of 62.9 % after 30 min. The recovery of the material is further limited at −60 °C and has only a CS of 82.5 % after 30 min, meaning the seal is mostly frozen and only very limited recovery is given. The released states after 30 min are shown at the bottom side of Fig. 12 and point out the time- and temperature dependency of the elastomeric seal and highlight the limited elastic recovery of elastomers at low temperature.

3.2.4. Stress relaxation

Stress relaxation of elastomers depends on time and temperature. If an elastomer is initially deformed to ε_0 and stays constant, the stress first increases to a high-level σ_0, then relaxes to a much lower level σ_∞ that can be much smaller than σ_0. Immediately after the initial deformation, the polymeric chains do not have enough time to react, and the elastomer behaves like a linear-elastic solid. The corresponding modulus is equivalent to the one of glass and is therefore termed glassy or instantaneous modulus E_0. After a long holding time, the modulus relaxes to the so-called static steady-state or equilibrium modulus E_∞. During this time, the molecular chains need time to reach their energetically preferred state, and stress relaxes.

Fig. 13 shows a uniaxial tensile specimen that is elongated at a rate of 500 mm/min up to a constant strain level of 85 % at three different temperatures. The true stress response is presented over 24 h and shows very little stress relaxation from 12.6 MPa to a constant value of 10.9 MPa after 10 min at +85 °C. At +23 °C, the stresses relax from 15.7 MPa to 12.2 MPa after 3 h, and there is little further relaxation. Otherwise, the relaxation process shows greater stress relaxation at −60 °C, where the stress relaxes from 136.4 MPa to 52.0 MPa after 3 h, 46.4 MPa after 12 h, and continues to relax further after this time. The elastomer needs more time to restructure its chains at low temperature, and hence, greater stress relaxation is given in comparison to higher temperatures.

An additional FE simulation was performed to identify these individual effects and their impact on the sealing performance. Therefore, a 21 % compressed axial O-ring (15.6 mm × 1.78 mm) is cooled from +20 °C to −80 °C, as shown in Fig. 14. A cooling rate of −1 °C/min is shown with and without considering thermal expansion in A, and three different cooling rates are compared in B.

Fig. 14A used FEA without any thermal expansion showing the effect of pure axial stress relaxation that is equal to the pressure at the contacts. The contact pressure relaxed from 3.40 MPa at 20 °C to 3.32 MPa at 7 °C staying constant even up to −80 °C (see yellow curve). If thermal shrinkage of the elastomeric seal is considered, the thermal expansion coefficient acts linearly when cooling (see green field) and reduces the cross-section diameter d_2. A pure hyperelastic FE simulation confirmed the linear reduction of contact pressure when cooling. Elastic recovery is needed to keep the contact pressure acting when considering the reduction of the O-ring thickness when cooling. As previously explained, this recovery is increasingly limited as the temperature is lowered, especially below −40 °C. Therefore, the contact pressure not only suffers under stress relaxation at the beginning and a linear thermal contraction. Instead, the elastic recovery becomes greatly weakened, and the contact pressure is exponentially weakened, as shown from −30 to −80 °C. These three significant effects highlight the impact of the materials in addition to the geometrical influences. The consideration of the worst-case machining tolerances would show a reduced offset of the contact pressure for the entire temperature range. Moreover, Fig. 14B compares the cooling rates of −1 °C/min, −10 °C/min, and −20 °C/min for the same axial compressed O-ring that is cooled from 20 °C to −80 °C. There seems to be no significant stress relaxation when cooling at a faster rate. However, the recovery is further limited, and the contact pressure is clearly reduced for the temperature range of −55 °C to −80 °C. At −80 °C, the recovery comes to rest for the cooling rate of −10 °C/min, and no contact pressure is given for the assembled state. For −20 °C/min, this happens even earlier at −79 °C.

Fig. 14 summarizes the essential effects and their interaction when cooling an installed elastomer O-ring seal. The seal shrinks more due to a higher thermal expansion coefficient and generates a geometric change that must be compensated by the elastomeric recovery of the seal. However, this recovery is exponentially weakened as well as the contact pressure when cooling. Stress relaxation and machining tolerances have a much lower impact.

3.3. Leakage simulation and testing

Many industrial applications use O-rings to seal high-pressure loaded systems. Therefore, a pressurized O-ring is simulated and tested in the following.

Physically, a hermetically sealed system does not exist. Therefore,

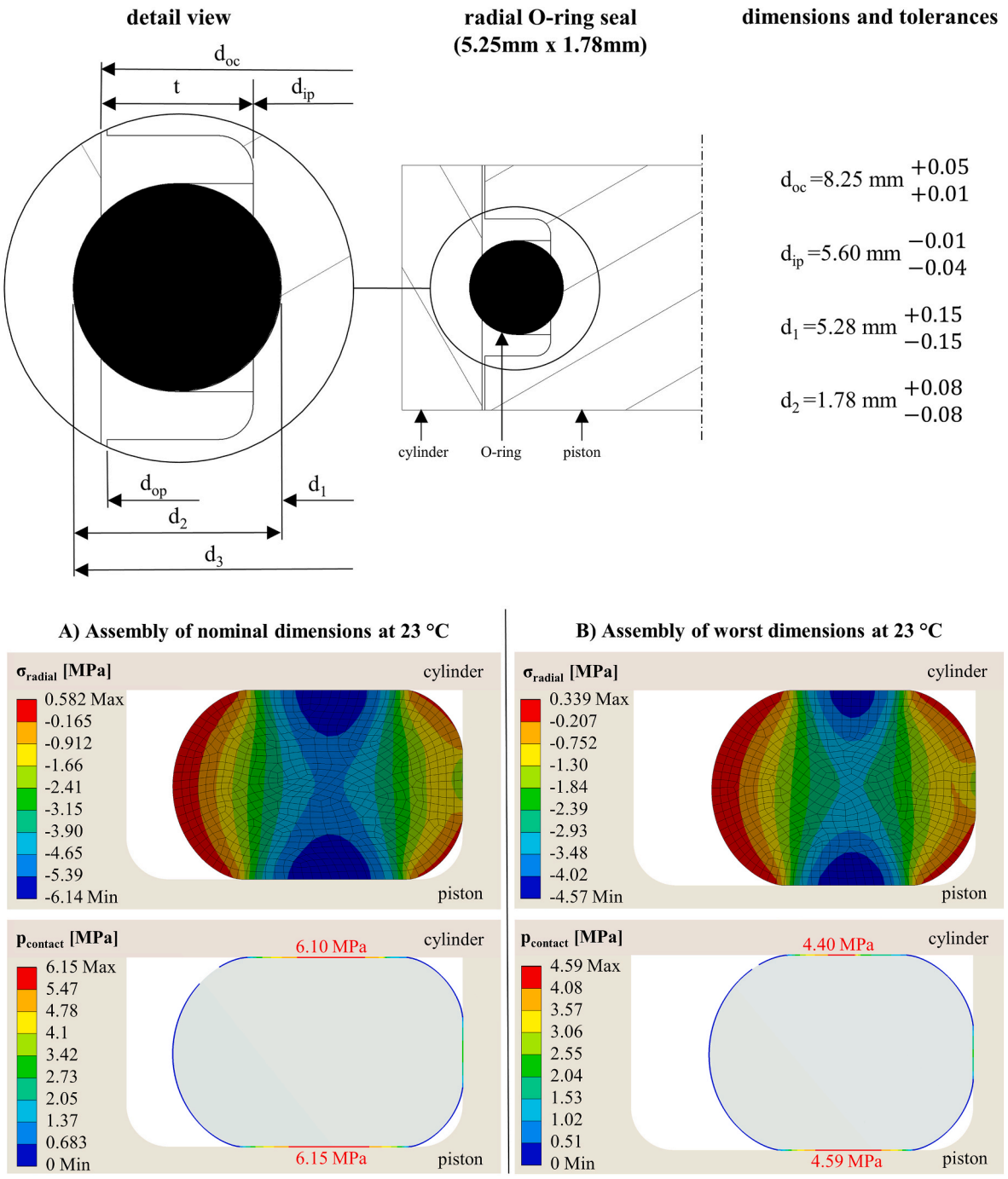

Fig. 11. Radial O-ring seal 5.28 x1.78 with tolerances and contact pressure.

the technical leak tightness is defined with regard to the specific operation [68]. This technical leak tightness is usually specified as an allowable leakage rate under maximum operating conditions. The required leak tightness can depend on the application. For example, a ring seal that does not show any visible oil leakage, like a drop, is generally defined as leak-proof but can have constant slight evaporation [2]. Contrarily, very low leakage rates are accepted for high-pressure applications, e.g. hydrogen storage systems. Here, the leakage volume of a medium is measured over time. The leakage rate quantifies the leakage of a sealing system and depends on the pressure difference and the quality of the materials. This indicator is defined with SI units in mbarl/s. That means 1mbarl/s presents the amount of gas that must be removed from a 1 L container in 1 s to decrease the pressure by 1 mbar.

Both primary and secondary leakage depend on the pressure difference Δp and move from the volume of higher pressure to the volume of lower pressure when considering a pure medium. A general measurement of the leakage rate does not differentiate between the two leakage types and hence, measures the resulting sum of both. Three different leakage measurements are typically used. A sniffer can detect external leakage close to the leak, but a more extensive and accurate method is a leak detector. This detector has a closed connection behind the seal, generates a vacuum, and measures the leakage rate with an integral method. A bubble test can be used for higher gaseous leakage rates. Franke [69] gives a detailed description of these leakage detection methods.

This leakage test investigates the leak tightness of a radially oriented O-ring 5.28 mm × 1.78 mm at Tg −60 °C. FE simulation and experiment

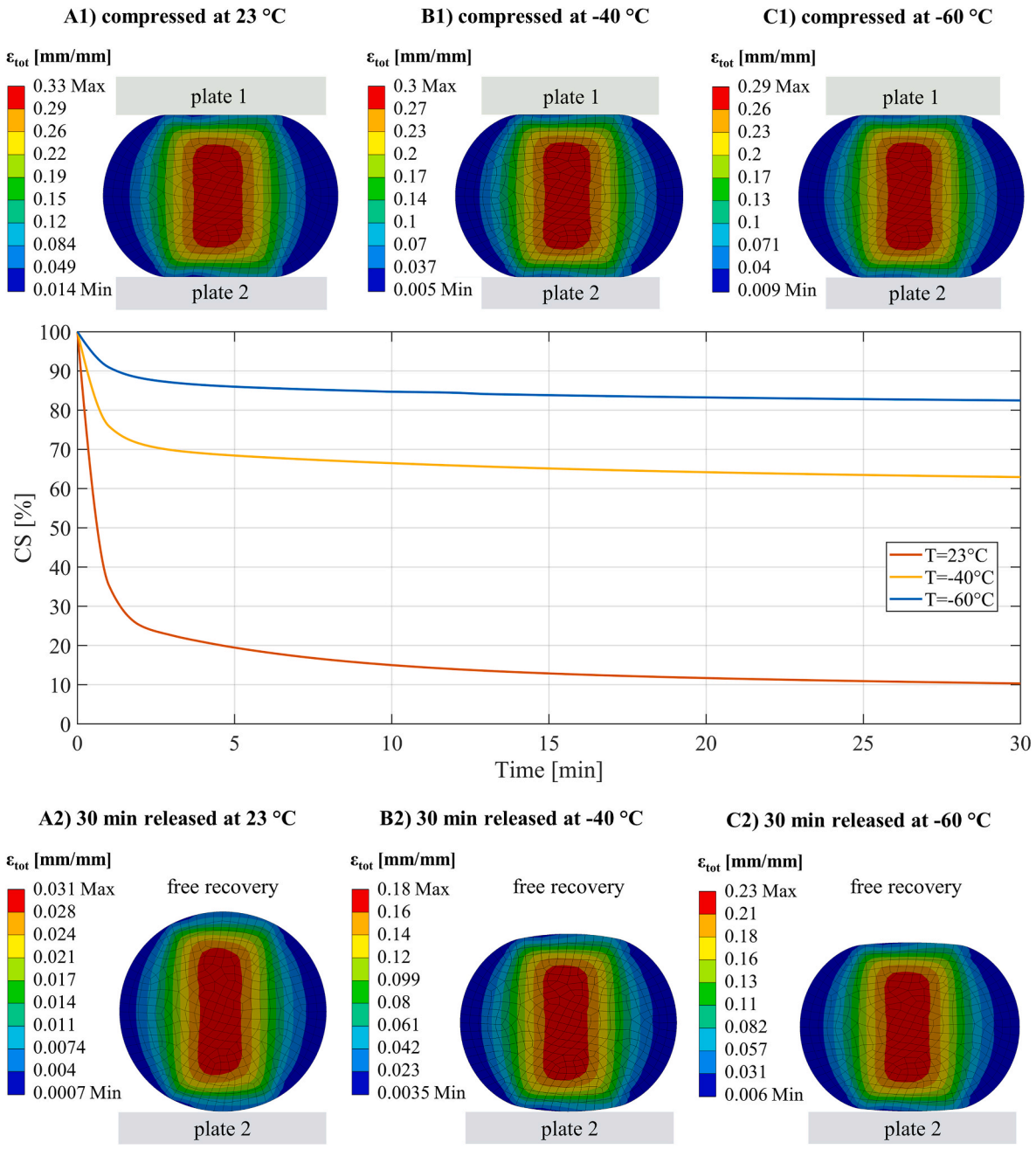

Fig. 12. Compression Set for O-ring 15.6 mm × 1.78 mm at: A) 23 °C; B) −40 °C; C) −60 °C.

were done without any back-up ring, which is typically used in practice to avoid extrusion, to focus purely on the sealing behavior of the elastomer O-ring. For the experiment, the pistons were made of Inconel 718, the cylinders of aluminum alloy EN AW 6082 T6, and the O-ring consisted of 80 FVMQ 567. The machining tolerances and surface conditions were checked before testing to ensure reliable test results. All machined metal components were cleaned in a heated ultrasonic bath (Fisherbrand FB15046). The O-rings were cleaned with isopropanol, and all contact faces were greased with gleitmo 595 to achieve better assembly through lower friction. A special assembly tool was designed and used to ensure good positioning of the O-ring during assembly. Finally, the parts were assembled and installed in a climate chamber (Vötsch Industrietechnik VT 7021) connected to a high-pressure test bench (MAXIMATOR).

The assembled specimen is connected to the high-pressure test bench on the left side in Fig. 15, and an additional tube is connected on the right side to measure the leakage rate with a leak detector (adixen ASM 142). The test setup was pre-conditioned at −60 °C for more than 2 h after reaching the test temperature in the climate chamber, as shown in Fig. 16A. The temperature was verified by an additional temperature sensor close to the seal. These experiments were performed at the ROTAREX laboratory using helium as its leakage rate can be converted to the one of hydrogen. If the measured leakage rate was above the minimum technical requirement ($q_{allowable} = 5\ 10^{-5}$mbarl/s), a bubble test was used to confirm high leakage rates. If bubbles occurred frequently, the leakage rate was far above the requirements. Afterward, a stepwise pressure ramping was done with approximately 10 bar/s to a constant pressure that was held for 1 min at each 100 bar step. The same procedure was done when decreasing the pressure. The test was stopped when high leakage occurred, and stable pressure could not be sustained.

Our test showed an acceptable leakage rate of 3.0 10^{-5}mbarl/s at 100 bar. When reaching 200 bar in the next step, big leakage occurred,

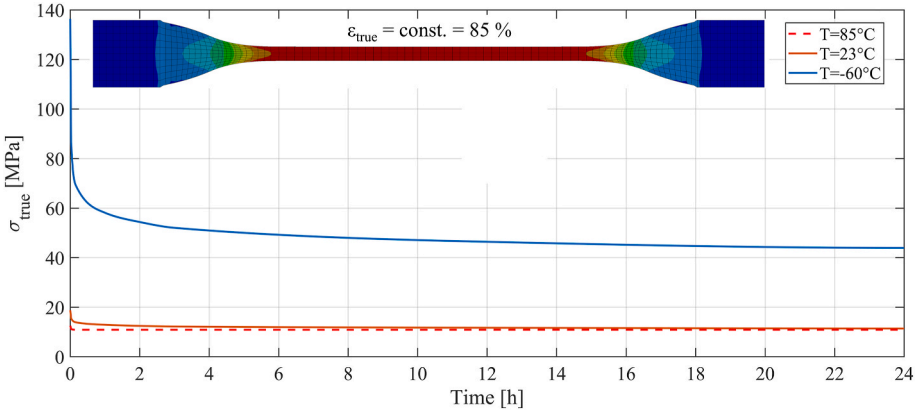

Fig. 13. Stress relaxation of a tensile specimen under constant strain at three temperatures.

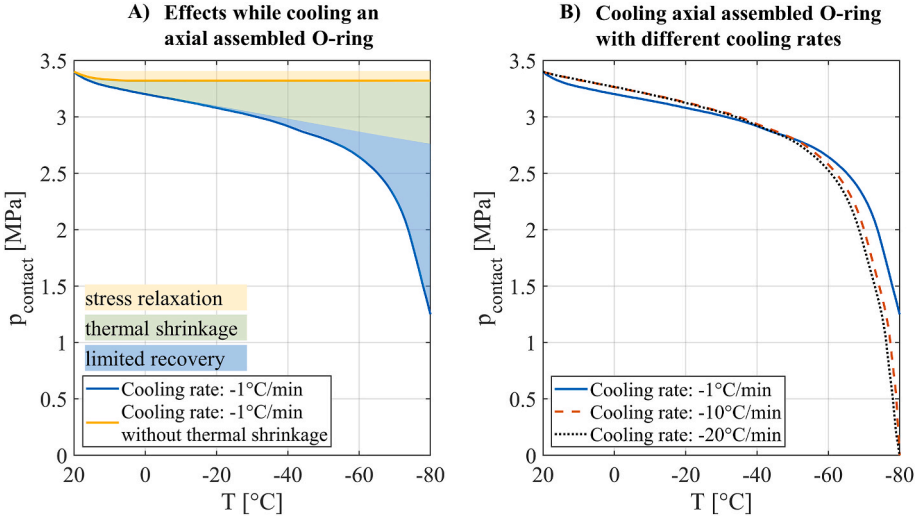

Fig. 14. Cooling of an axial assembled O-ring (15.6 x1.78): A) with and without thermal shrinkage; B) with different cooling rates.

confirmed by the bubble test and highlighted in Fig. 16. The same happened when trying to reach higher pressures. When reducing the pressure again to 100 bar, the system was leak-proof again with an acceptable leakage rate of 3.0 10^{-5}mbarl/s as before. The O-ring was checked after low-temperature testing and did not show any extrusion that could also be confirmed by FEA, as shown in Fig. 16B.

The FE simulations of radial O-rings were done in four load steps close to the experiment. First, the O-ring is stretched on the piston. Afterward, the piston with the O-ring is assembled into the cylinder (assembly). Third, the temperature can be reduced to the required minimum of −60 °C. Finally, the pressure can be increased to its maximum value by using the fluid pressure penetration in ANSYS which accounts for the effect of fluid penetration between seals and other structural components. The defined load pressure is linked to the contact set and a solver iteratively compares the fluid pressure and contact stress to determine the pressure-loaded area. The load-dependent deformations are iteratively updated and considered, especially for the O-ring.

It shows a generation of a leakage gap at only 200 bar, and a leakage occurred at 290 bar, where the contact pressure is below operating pressure. This leakage continues through continuous increase in pressure. Numerical results agree quite well with the experimental measurements. The appearance of leakage could be simulated at 290 bar, whereas the experiments showed leakage at 200 bar. As shown in Fig. 16, the contact pressure is unstable after leakage occurs. This behavior also occurred during several leakage tests where the seal seemed to close the gap again shortly. The phenomena of restructuring material recovery and changing contact conditions may explain this behavior. This highlights the complex behavior of the seal where the elastomer tries to counteract the gap generation. However, if leakage occurs the first time all higher operating pressures generally lead to leakage. Therefore, the first occurrence of a lower contact pressure than operating pressure is defined as the criterion of leakage within FEA simulation.

4. Discussion and conclusion

Most FE simulations match well with experimental results. However, some deviations could be reduced by further improving the overall model and simulation. Further material characterization tests (biaxial, shear), a higher-order hyperelastic material model, non-linear viscoelasticity, and the consideration of incompressibility could further improve the numerical results. Temporary high-temperature events can occur (e.g. +115 °C at 2.5 g/s flow rate) and have not been addressed in this work but should be investigated in future studies. Anyway, the essential influences and their impacts on low-temperature sealing tightness of an elastomer O-ring were detected and explained.

The understanding and correct material modeling for nonlinear elastomers is the bottom line for efficient development, optimization, construction, and application of elastomeric sealing products. This article gives a detailed description of the TRS viscoelastic material model that is used for FEA and matches well with several material tests for 80 FVMQ 567. Temperature Retraction, Compression Set, and even

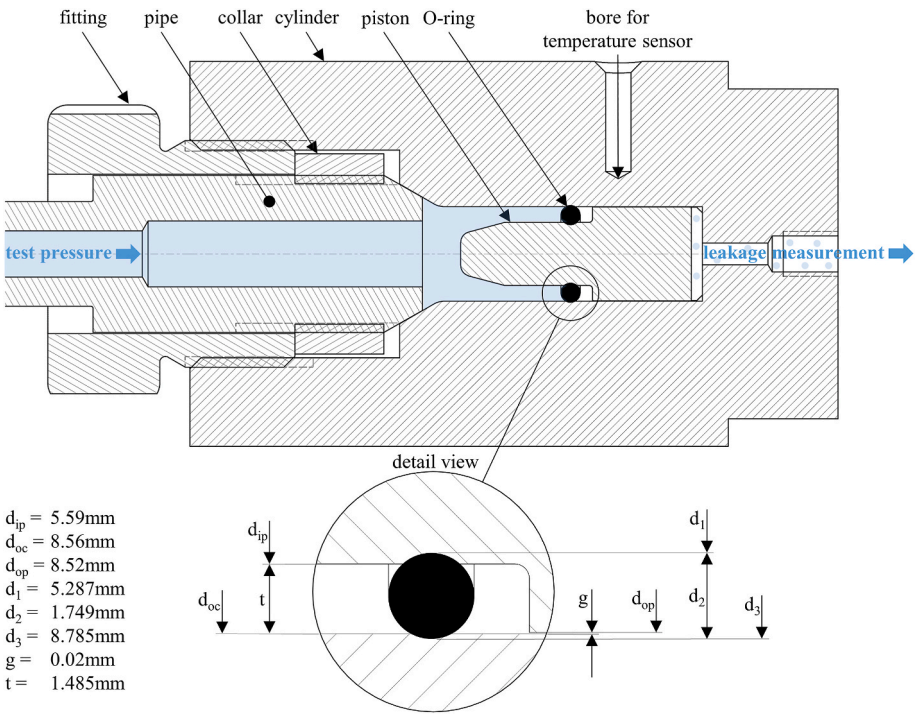

Fig. 15. Section view of installed specimen with measured dimensions.

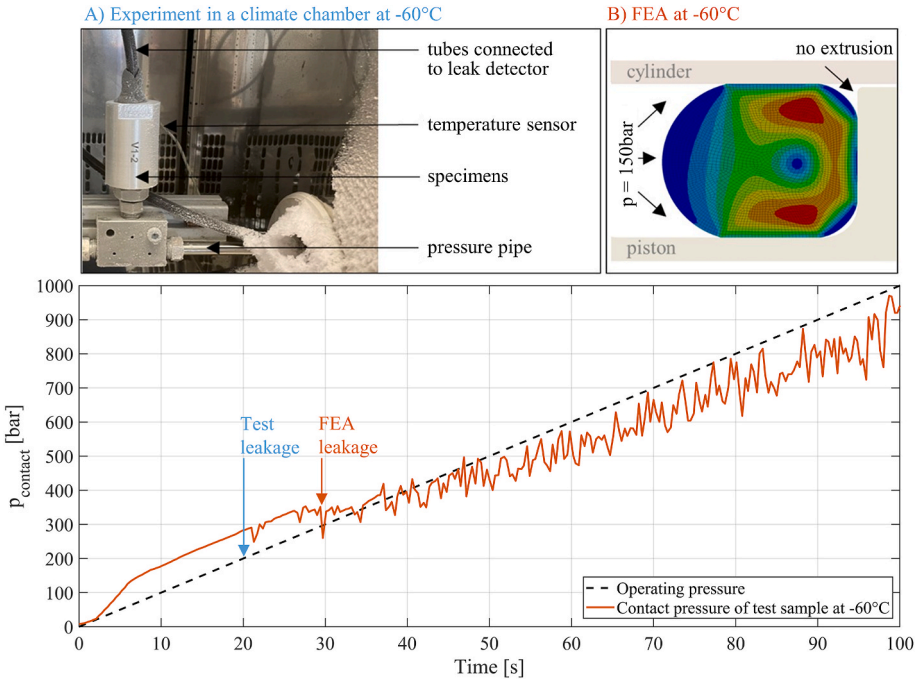

Fig. 16. Pressure load of cooled radial assembled O-rings at −60 °C in: A) Experiment and B) FEA.

pressure-loaded leakage tests were simulated and confirmed by real experiments. The generation of leakage could be shown as well. FEA could identify and segregate the essential effects being responsible for primary leakage at low temperature and the limitation of elastomers. When cooling, higher thermal shrinkage of the elastomer compared to its metal housing leads to a linear proportional reduction of the contact pressure due to geometrical changes and needs direct elastic recovery to counteract this geometrical change. However, this elastic recovery is limited ever stronger when reaching lower temperatures, especially close to T_g. Stress relaxation has an additional time-dependent impact when considering specific temperatures and load conditions. The consideration of machining tolerances could even accelerate the generation of leakage, e.g. lower contact pressure or unfavorable surface conditions. Finally, thermal shrinkage and limited elastic recovery interact when cooling and are mainly responsible for the occurrence of primary leakage.

CRediT authorship contribution statement

C. Repplinger: Writing – review & editing, Writing – original draft, Visualization, Validation, Software, Methodology, Investigation, Formal analysis, Data curation, Conceptualization. **S. Sellen:** Writing – review & editing, Supervision, Resources, Project administration, Methodology, Funding acquisition. **S. Kedziora:** Writing – review & editing, Supervision, Methodology. **A. Zürbes:** Writing – review & editing, Supervision. **S. Maas:** Writing – review & editing, Supervision, Project administration, Methodology, Investigation.

Declaration of competing interest

The authors declare that they have no known competing financial interests or personal relationships that could have appeared to influence the work reported in this paper.

Acknowledgments

The present work was supported and funded by the company ROTAREX S.A. for research on high-pressure valves with the main focus on the sealing behavior of elastomer O-rings at low temperature.

Nomenclature

a_T	time-temperature shift factor [−]
C_{ij}	hyperelastic material constant [−]
C_1	material constant of WLF-shift [−]
C_2	material constant of WLF-shift [°C]
CS	Compression Set [%]
D_1	incompressibility factor [1/MPa]
dev_{rel}	relative deviation [−]
DMTA	Dynamic Mechanical Thermal Analysis
DSC	Differential Scanning Calorimetry
d	diameter [mm]
E	modulus of elasticity [MPa]
E'	storage modulus [MPa]
E″	loss modulus [MPa]
E*	complex modulus [MPa]
E_0	instantaneous or glassy modulus [MPa]
E_∞	equilibrium modulus [MPa]
e_i	relaxation coefficient [−]
f	frequency [Hz]
FEA	Finite Element Analysis
FCEV	Fuel Cell Electric Vehicle
G	shear modulus [MPa]
I_i	deformation invariants [−]
J	elastic volume ratio [−]
J_m	limiting value [−]
K	bulk modulus [MPa]
L	length [mm]
L_0	length of unstretched specimen [mm]
L_e	length of stretched specimen [mm]
L_t	length of specimen at any observed temperature [mm]
NWP	nominal working pressure [bar]
OTV	on-tank valve
p	pressure [bar]
$p_{contact}$	contact pressure [MPa]
q	leakage rate [mbarl/s]; [ml/h]
R	stress ratio [−]
Ra	surface roughness [μm]
T	temperature [°C]; [K]
T_g	glass transition temperature [°C]; [K]
TR	Temperature Retraction [%]
TTSP	Time-Temperature Superposition Principle
t	time [s; min; h]
tan δ	loss factor [−]
V	volume [m^3]
W	strain-energy function [MPa]
WLF	Williams-Landel-Ferry shift function
$\|X\|_F$	Frobenius norm [−]
α_i	hyperelastic material constant [−]
α_{th}	thermal expansion coefficient [1/K]
δ	phase angle [°]
ε	strain [mm/mm]
η	viscosity [Ns/m^2]
λ_i	stretch [−]
μ_i	material constant [−]
ν	Poisson's ratio [−]
σ	stress [MPa]
τ_i	relaxation time [s]
ω	angular frequency [1/s]

References

[1] Szabó G, Váradii K. Large strain viscoelastic material model for deformation, stress and strain analysis of O-ring. Period Polytech - Mech Eng 2018;62:148–57.
[2] W. Haas, "Grundlehrgang Dichtungstechnik," Institut für Maschinenelemente (IMA) - Universität Stuttgart.
[3] Grelle T, Wolff D, Jaunich M. Temperature-dependent leak tightness of elastomer seals after partial and rapid release of compression. Polym Test 2015;48:44–9.
[4] H. K. Müller and B. S. Nau, "Grundbegriffe der Dichtungstechnik," www.fachwissendichtungstechnik.de.
[5] "Commission Regulation (EU) No. 406/2010, Implementing regulation (EC) No 79/2009 of the European Parliament and of the Council on type-approval of hydrogen-powered motor vehicles.". Off J Eur Union 2010.
[6] Albrecht D, Achenbach M. Seals for high-pressure tank systems in fuel cell cars. In: KGK rubberpoint; 2014.
[7] Thomson W, Joule JP. Ueber die Wärmewirkung bewegter Flüssigkeiten. Annalen der Physik und Chemie 1856;173:576–89.
[8] Chen J, Veenstra M, Purewal J, Hobein B, Papasavva S. Modeling a hydrogen pressure regulator in a fuel cell system with Joule–Thomson effect. Int J Hydrogen Energy 2019;44:1272–87.
[9] Toyota launches the new Mirai," www.global.toyota, February. 23, 2021.
[10] Merkle S, Achenbach M. Das müssen Sie bei der Berechnung von Gummi unbedingt wissen. In: Ingenieurbüro merkle & partner/stefan merkle holding GmbH, heidenheim; 2018.
[11] Jaunich M. Tieftemperaturverhalten von Elastomeren im Dichtungseinsatz. Berlin: BAM - Bundesanstalt für Materialforschung und -prüfung; 2012. Dissertation.
[12] Battermann W, Köhler R. Elastomere Federung, elastische Lagerungen: Grundlagen ingenieurmäßiger Berechnung und Konstruktion. Ernst & Sohn; 1982.
[13] Lutz T. Ein Beitrag zur Berechnung druckbelasteter Elastomerlager. Universität Kaiserslautern; 1990. Dissertation.
[14] Holzapfel GA. Nonlinear solid mechanics: a continuum approach for engineering. Chichester: John Wiley & Sons Ltd; 2000.
[15] Bonet J, Wood RD. Nonlinear continuum mechanics for finite element analysis. New York: Cambridge University Press; 2008.
[16] Stommel M, Stojek M, Korte W. FEM zur Berechnung von Kunststoff- und Elastomerbauteilen. München: Carl Hanser Verlag; 2011.
[17] Treloar LRG. The elasticity of a network of long-chain molecules - II. Trans Faraday Soc 1943;39:241–6.
[18] Mooney M. A theory of large elastic deformation. J Appl Phys 1940;11:582–92.
[19] Rivlin RS, Saunders DW. Large elastic deformations of isotropic materials. VII. Experiments on the deformation of rubber. Phil Trans Roy Soc Lond Math Phys Sci 1951;243:251–88.
[20] Yeoh OH. Characterization of elastic properties of carbon-black-filled rubber vulcanizates. Rubber Chem Technol 1990;63:792–805.
[21] Ogden RW. Large deformation isotropic elasticity - on the correlation of theory and experiment for incompressible rubberlike solids. Proceedings of the Royal Society of London. A. Mathematical and Physical Sciences 1972;326:565–84.
[22] Gent AN. A new constitutive relation for rubber. Rubber Chem Technol 1996;69:59–61.
[23] Fillers RW, Tschoegl NW. The effect of pressure on the mechanical properties of polymers. Trans Soc Rheol 1977;21:51–100.
[24] Moonan WK, Tschoegl NW. Effect of pressure on the mechanical properties of polymers. 2. Expansivity and compressibility measurements. Macromolecules 1983;16:55–9.
[25] Moonan WK, Tschoegl NW. Effect of pressure on the mechanical properties of polymers. 3. Substitution of the glassy parameters for those of the occupied volume. International Journal of Polymeric Materials and Polymeric Biomaterials 1984;10:199–211.
[26] Kralj A, Prodan T, Emri I. Review on effect of pressure on mechanical properties of polymers and apparatus for measurements under hydrostatic pressure. 1999. p. 1–28.
[27] Ferry JD. Viscoelastic properties of polymers. New York: John Wiley & Sons, Inc; 1980.

[28] Ho E. Elastomeric seals for rapid gas decompression applications in high-pressure services. Cranfield: BHR group, The Fluid Engineering Centre; 2006.
[29] ISO 37. Rubber, vulcanized or thermoplastic - determination of tensile stress-strain properties. 2017.
[30] Hooke R. Lectures de potentia restitutiva, or of spring explaining the power of springing bodies. In: John martyn; 2024. London.
[31] Newton I. The mathematical principles of natural philosophy. In: College of physicians, and of the. London: Royal Society; 2024.
[32] Czibula C, Ganser C, Seidlhofer T, Teichert C, Hirn U. Transverse viscoelastic properties of pulp fibers investigated with an atomic force microscopy method. J Mater Sci 2019;54:11448–61.
[33] Schuster M, Kraus M, Schneider J, Siebert G. Investigations on the thermorheologically complex material behaviour of the laminated safety glass interlayer ethylenevinyl-acetate, 3; 2018. p. 373–88.
[34] Kelly P. Solid mechanics Part I: an introduction to solid mechanics. University of Aukland; 2013.
[35] Hearn EJ. Miscellaneous topics. In: Mechanics of materials, 2; 1997. p. 509–33.
[36] Rust W. Nichtlineare finite-elemente-berechnungen: kontakt, geometrie, material. Wiesbaden: Vieweg + Teubner Verlag; 2011.
[37] Tobolsky AV. Stress relaxation studies of the viscoelastic properties of polymers. J Appl Phys 1956;27:673–85.
[38] Brostow W, Menard KP, White JB. Application of dynamic mechanical analysis techniques to bismuth telluride based thermoelectric materials. E-Polymers 2004; 45:1–13.
[39] Vives AA. Piezoelectric tansducers and applications. Berlin, Heidelberg: Springer Verlag; 2008.
[40] Schwarzl FR. *Polymermechanik*. Erlangen. Springer-Verlag; 1990.
[41] Li. Time-temperature superposition method for glass transition temperature of plastic materials. Mater Sci Eng 2000;278:36–45.
[42] Nakano T. Applicability condition of time-temperature superposition principle (TTSP) to a multi-phase system. Mech Time-Dependent Mater 2013;17:439–47.
[43] Herdy M. Introductory theory manual - ViscoData & ViscoShift. 2003.
[44] Williams ML, Landel RF, Ferry JD. The temperature dependence of relaxation mechanisms in amorphous polymers and other glass-forming liquids. J Am Chem Soc 1955;77:3701–7.
[45] Michaeli W, Brandt M, Brinkmann M. Simulation des nicht-linear viskoelastischen Werkstoffverhaltens von Kunststoffen mit dem 3D-Deformationsmodell. Zeitschrift Kunststofftechnik/Journal of Plastics Technology 2006;2:1–24.
[46] Peschke H. Simulation von Elastomerdichtungen unter dynamischer Belastung. In: INA-Sonderdruck; 1999. p. 1–7.
[47] Achenbach M, Streit G. Thermodynamische Beschreibung der Gummielastizität. In: 11. International sealing conference. Dresden; 1999. p. 1–16.
[48] Kraus M, Schuster M, Kuntsche J, Siebert G, Schneider J. Parameter identification methods for visco- and hyperelastic material models. Glass Structures & Engineering 2017;2:147–67.
[49] Akulichev AG, Echtermeyer AT, Persson BNJ. Interfacial leakage of elastomer seals at low temperatures. Int J Pres Ves Pip 2018;160:14–23.
[50] Rouleau L, Pirk R, Pluymers B, Desmet W. Characterization and modeling of the viscoelastic behavior of a self-adhesive rubber using dynamic mechanical analysis tests. J Aero Technol Manag 2015;7:200–8.
[51] Bargel HJ, Schulze G. Werkstoffkunde. Berlin: Springer; 2005.
[52] Rinnbauer M. Technische Elastomerwerkstoffe: Basis für Hightech-Lösungen in der Dichtungs- und Schwingungstechnik. Weinheim: Verlag Moderne Industrie/ Freudenberg Sealing Technologies GmbH & Co. KG; 2006.
[53] Achenbach M. Service life of seals – numerical simulation in sealing technology enhances prognoses. Comput Mater Sci 2000;19:213–22.
[54] Grelle T, Wolff D, Jaunich M. Leakage behaviour of elastomer seals under dynamic unloading conditions at low temperatures. Polym Test 2017;58:219–26.
[55] Ehrenstein GW, Riedel G, Trawiel P. Thermal analysis of plastics. München: Carl Hanser Verlag GmbH & Co. KG; 2004.
[56] Abubakar IJ, Myler P, Zhou E. Constitutive modelling of elastomeric seal material under compressive loading. In: Modeling and numerical simulation of material science, 6; 2016. p. 28–40.
[57] Popov VL. Kontaktmechanik und Reibung - Von der Nanotribologie bis zur Erdbebendynamik. Berlin: Springer Vieweg; 2015.
[58] Kraus M, Niederwald M, Siebert G, Keuser M. Rheological modelling of linear viscoelastic materials for strengthening in bridge engineering. In: *Japanese German bridge symposium*, osaka; 2016. p. 1–12.
[59] Gordnian K. Crystallization and thermo-viscoelastic modelling of polymer composites. Vancouver: University of British Columbia; 2017. Dissertation.
[60] ISO 2921. Rubber, vulcanized - determination of low-temperature characteristics - temperature-retraction procedure (TR test). 2019.
[61] Akulichev AG, Alcock B, Echtermeyer AT. Elastic recovery after compression in HNBR at low and moderate temperatures: experiment and modelling. Polym Test 2017;61:46–56.
[62] Jaunich M, Stark W, Wolff D. A new method to evaluate the low temperature function of rubber sealing materials. Polym Test 2010;29:815–23.
[63] Jaunich M, Stark W, Wolff D. Comparison of low temperature properties of different elastomer materials investigated by a new method for compression set measurement. Polym Test 2012;31:987–92.
[64] ISO 3601-1: fluid power systems - O-rings - Part 1: inside diameters, cross-sections, tolerances and designation codes. 2012.
[65] Cerbe G, Wilhelms G. Technische Thermodynamik - Theoretische Grundlagen und praktische Anwendungen. München: Carl Hanser Verlag; 2011.
[66] Hornig R, Sunder J. Low-temperature sealing force behaviour of FKM elastomers as a function of the degree of chemical crosslinking and cifferently restricted geometric deformation in static compression. Int Polym Sci Technol 2015;42:1–10.
[67] DIN ISO 815-2: Rubber. Vulcanized or thermoplastic - determination of compression set - Part 2: at low temperatures. 2016.
[68] Li H, Ma J, Liu BY, Gu RJ, Li GJ. An insight into neutral layer shifting in tube bending. Int J Mach Tool Manufact 2018;126:51–70.
[69] H. Franke, “Seminar über Dichtheitsmessungen und Lecksuchmethoden,” www.lecksuchtechnik.de.